IEEE Journal of Translational Engineering in Health and Medicine

Received 19 February 2024; revised 31 August 2024; accepted 3 September 2024.
Date of publication 10 September 2024; date of current version 26 September 2024.

Digital Object Identifier 10.1109/JTEHM.2024.3457593

A Pre-Voiding Alarm System Using Wearable Ultrasound and Machine Learning Algorithms for Children With Nocturnal Enuresis

JUN WANG[1], (Graduate Student Member, IEEE), ZEYANG DAI[1], AND XIAO LIU[1,2,3], (Senior Member, IEEE)

[1]School of Information Science and Technology, Fudan University, Shanghai 200433, China
[2]State Key Laboratory of Integrated Chips and Systems, Fudan University, Shanghai 201203, China
[3]Greater Bay Area Institute of Precision Medicine, Guangzhou 511400, China

CORRESPONDING AUTHOR: X. LIU (xiao@fudan.edu.cn)

This work was supported in part by STI 2030-Major Projects under Grant 2022ZD0208900, in part by the Science and Technology Commission of Shanghai Municipality under Grant 20S31903800, in part by NSFC under Grant 62150610498, in part by Shanghai Municipal Science and Technology Major Project under Grant 2021SHZDZX, and in part by the Greater Bay Area Institute of Precision Medicine (Guangzhou).

ABSTRACT Nocturnal enuresis is a bothersome condition that affects many children and their caregivers. Post-voiding systems is of little value in training a child into a correct voiding routing while existing pre-voiding systems suffer from several practical limitations, such as cumbersome hardware, assuming individual bladder shapes being universal, and being sensitive to sensor placement error. Methods: A low-voltage ultrasound system with machine learning has been developed in estimating bladder filling status. A custom-made flexible 1D transducer array has been excited by low-voltage coded pulses with a pulse compression technique for an enhanced signal-to-noise ratio. In order to minimize the negative influence of possible transducer misplacement, a multiple-position training strategy using machine learning has been adopted in this work. Three popular classification methods, KNN, SVM and sparse coding, have been utilized to classify the acquired different volumes ranging from 100 ml to 300 ml into two categories: low volume and high volume. The low-volume category requires no further action while the high-volume category triggers an alarm to alert the child and caregiver. Results: When the sensor placement is ideal, i.e., the position of the practical sensor placement is on spot with the trained position, the precision and recall of the classification using sparse coding are 0.957 ± 0.02 and 0.958 ± 0.02, respectively. Even if the transducer array is misplaced by up to 4.5 mm away from the ideal location, the proposed system is able to maintain high classification accuracy (precision ≥ 0.75 and recall ≥ 0.75). Category: Early/Pre-Clinical Research

INDEX TERMS Bladder filling status, bladder volume, machine learning, sparse coding, ultrasound system, wearable system.

Clinical and Translational Impact: The proposed ultrasound sensor system for nocturnal enuresis is of significant clinical and translational value as it addresses two major issues that limit the wide adoption of similar devices. Firstly, it offers enhanced safety as the entire system has been implemented in the low-voltage domain. Secondly, the system features ample tolerance to sensor misplacement while maintaining high classification accuracy. These features combined provide a much more user-friendly environment for children and their caregivers than existing devices.

I. INTRODUCTION

NOCTURNAL enuresis (NE) is the involuntary voiding of urine during sleep that occurs at least twice a week in children aged five years or above, according to the definition from the International Child Continence Society (ICCS) [1]. It is a devastating condition in children that affects their quality of life and emotional well-being. Approximately 5% to 10% of children suffer from NE worldwide. In China, 7.3% of children and adolescents suffer from NE, and this prevalence has been on an increasing trend over the recent

years [2]. Although the majority of children will outgrow the condition, the persistence of NE can lead to negative psychosocial outcomes, including decreased self-esteem, social isolation, and anxiety [3].

There are several treatment options for NE, including medications, behavioral therapies, and sensor-based alarm interventions. Desmopressin is a drug commonly used in the treatment of NE and has a significant clinical response rate. But it is also associated with about 65% relapse rate and some undesirable side effects, such as dizziness, anorexia and vomiting [4]. Urotherapy is a behavioral therapy which involves implementing straightforward interventions such as restricted fluid intake and educating individuals on optimizing voiding patterns through lifestyle adjustment. These interventions are known for their simplicity and have little side effects. However, persistent behavioral therapy can be very demanding for children, and low compliance may lead to low effectiveness [5].

Sensor-based bedwetting alarm systems have minimal side effects and do not cause dependency, making them to be the first-line treatment for children with NE in the guidelines of ICCS [6]. Commercially available bedwetting alarm systems rely on a humidity sensor which has been embedded into a child's undergarment. When the child starts to urinate, the increased wetness of the undergarment is detected and triggers the alarm, waking up the child and caregiver. However, such a post-voiding alarm occurs after the child has started urinating. Despite their simplicity and effectiveness in reporting a bedwetting event, humidity sensor-based alarm systems fail to provide pre-voiding warnings. Post-voiding alarms have little use in training a child to develop reflexive control mechanism of micturition [7], [50]. In addition, post-voiding alarm systems do not change the fact that the quality of sleep for both the child and his/her caregiver is significantly affected by the burdensome routing, i.e., changing the child's diaper and possibly changing the child's wet clothes and beddings at midnight.

In recent years, many non-invasive sensor-based monitoring techniques, such as near-infrared spectroscopy (NIRS), electrical impedance tomography (EIT), and ultrasound (US), have been applied to the field of bladder monitoring with the common goal of producing a pre-voiding alert. NIRS can estimate the increase in bladder volume by detecting the absorption of infrared light by different urine volumes at specific wavelengths [8]. However, NIRS can potentially cause skin damage if a child is exposed to infrared light for a prolonged period of time [9]. EIT can determine bladder filling status by employing an electrode belt which is placed along the perimeter of the lower abdomen of a user. It detects impedance distribution and conductivity variations within the perimeter of the electrode belt. The changing impedance is a useful indicator for the variation of the bladder volume. An EIT device typically requires more than 16 electrodes to encircle the pelvis region [10] in order to obtain the bladder shape information on the transverse plane. However, such an all-around electrode belt is sensitive to body movements and is uncomfortable to wear at night. US is a well-established clinical technique for imaging the inner human organs. Clinical US imaging devices operating in the brightness mode (B-Mode) have demonstrated sufficient accuracy in estimating bladder volumes [11], [12]. A B-Mode US image consists of hundreds of pixels whose brightness correlates to the amplitude of reflected echo signals. Bladder tissue and urine have very different acoustic impedance, causing ultrasound waves to reflect at the tissue-urine interface. Hence, the boundaries between the bladder tissue and urine are evident on a B-mode US image, illustrating the physical shape of a bladder. With a standard B-mode ultrasound (US) device, the information on the height (H), width (W), and depth (D) of a bladder can be extracted. The height is determined from the maximum vertical distance between the bladder walls in a sagittal-plane image, the width from the maximum horizontal distance between the bladder walls in a transverse-plane image, and the depth from the maximum horizontal distance between the bladder walls in a sagittal-plane image. Assuming a bladder is of an ellipsoid shape, its volume can be calculated by the following empirical equation [13]:

$$\text{Volume(ml)} = 0.52 \times H(\text{cm}) \times W(\text{cm}) \times D(\text{cm}) \quad (1)$$

Although a clinical B-mode US device has been considered as a reliable tool for bladder scanning and volume estimation, the equipment itself is bulky and expensive. To cover a wide viewing angle so the entire bladder is within the vision, a US probe with 128 or more transducer elements is usually required in a B-mode US system. The high number of transducer elements significantly increases system complexity and cost, limiting its usage to business users, such as those being used in clinics. To meet the low-cost need of usage in a home environment, portable US devices working in the amplitude mode (A-mode) have been proposed. An A-mode US device determines the positions of a bladder's posterior and anterior walls by measuring the amplitude and time of flight (TOF) of echoed US signals. While a B-mode US system is able to show the physical shape of an entire bladder, an A-mode US system describe a bladder using limited numbers of dots. Hence, an A-mode system trades the measurement accuracy for cost. Using a single transducer placed on the lower abdomen, as shown in Fig. 1(a), Van Leuteren et al. found a correlation between the depth of anterior-posterior (A-P) walls and the volume of a bladder in a urodynamic study consisting of 30 children [14]. Despite its simple structure, the bladder monitoring relied on only one transducer and a slight position change of the transducer could cause significant measurement error. In Fig. 1(b), Niu et al. employed a linear array of transducers to scan the bladder in the sagittal plane [15]. The maximum depth, $D_{\max}$, was chosen among a group of distances between anterior and posterior walls measured by transducers at different heights. The height, H, was decided by the vertical height difference between the highest and lowest transducers to which the bladder was visible. The bladder volume was then estimated by the following

IEEE Journal of Translational Engineering in Health and Medicine

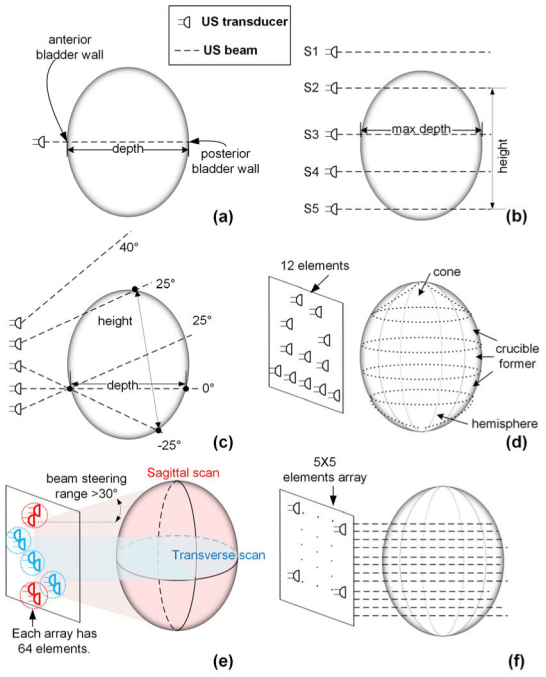

FIGURE 1. Existing wearable US systems for bladder volume monitoring.

empirical equation [16]:

$$\text{Volume (ml)} = 7.1 \times H\ \text{(cm)} \times D_{\max}\ \text{(cm)} - 23 \quad (2)$$

A linear transducer array offers more accurate measurement on the bladder volume and is less sensitive to transducers' placement errors than a single transducer. However, its estimation on the bladder volume is based on the assumption of a bladder shape following a simple geometric model, such as a sphere or ellipsoid. In practice, bladder shapes vary on an individual basis and cannot be assumed to be generic. Palanchon et al. proposed a US monitoring system that employed five transducers with predetermined angles [17], as shown in Fig. 1(c). One sound beam was oriented perpendicularly to the bladder anterior wall (denoted as 0°), while other four beams were fixed at −25°, 25°, 25°, 40° to estimate the depth, D, and height, H, of the bladder. Different bladder shapes and volumes were visible to different transducers. Depending on the set of transducers involved in the measurement, the system had a sophisticated algorithms in deciding the exact depth and height. Finally, the bladder volume was calculated by:

$$\text{Volume (ml)} = k \times H\ \text{(cm)} \times D\ \text{(cm)} \quad (3)$$

where k is a coefficient determined through linear regression analysis of the experimental data. An experiment involving 33 volunteers demonstrated that the average error using this method was approximately 12.5% [17]. Tanaka et al. reconstructed a bladder image by cumulative fitting of multiple cones, crucibles, and hemispheres [18], as depicted in Fig. 1(d). Therefore, the total volume of the bladder was the sum of the individual volumes from separable parts. In a trial based on 61 volunteers with bladder volumes ranging from 44 ml to 506 ml, the estimated volumes using this method showed good agreement (correlation coefficient $r = 0.98$) with the actually voided volumes. Using this method, the arrangement of individual US elements in the transducer array and the exact position of the array's placement are two major factors that affect the accuracy of the measurement. In Fig. 1(e), Zhang et al. utilized five phase arrays each of which consists of 64 US transducer elements [42]. Each phase array has a beam steering range greater than 30°. The five phase arrays were placed in a cross arrangement, capable of scanning both the transverse and sagittal planes without the need for manually rotating the US patch. After acquiring the bladder images in the transverse and sagittal planes, the length, width and height of the bladder, which were the key factors for estimating the bladder volume, were extracted from the images. A human clinical study using this method showed only $-3.2 \pm 6.4\%$ mean error in estimating bladder volume when being compared a reference clinical system. A similar design but with a different transducer array configuration was presented in [19]. The generation of US images from phase arrays usually demands substantial computational resources, leading to reduced battery time due to high power consumption. In addition, the high cost of phase-array transducers hinders its widespread applications in wearable devices. In 2021, Jo et al. designed a wearable bladder scanner system consisting of 25 standalone transducers embedded in a 5 × 5 matrix [20], as shown in Fig. 1(f). In contrast to the phase array in Fig. 1(e) which had a steerable range, the 25-transducer matrix in Fig. 1(f), could only send acoustic signals in a predefined direction with no beam-steering capability. An ellipsoid fitting algorithm was utilized to estimate the volume based on the acquired spatial information. In an experiment using a porcine bladder submerged in a water tank, the device had a mean error of 24 ml when the expected bladder volume ranged from 50 ml to 450 ml.

In the aforementioned wearable US systems, the bladder shape was often approximated as a simple ellipsoid or sphere. However, according to a research study including 146 children, bladder shapes have been categorized as sphere, ellipsoid, cuboid and pyramid among which ellipsoid and sphere take account for less than half of the total sample size [21]. The practical bladder shape can have a significant impact on the accuracy of bladder volume estimation. Machine learning (ML) is a useful tool to obtain an accurate estimation of the bladder filling status by training a large number of samples without relying on any pre-determined hypothetical geometric bladder shape or any specific mathematical equations for calculating the volume. Kuru et al. used ML methods to determine bladder filling status and to trigger a pre-voiding alarm when the bladder volume reaches three quarters of the maximum fullness [22]. The reported sensitivity and specificity values were 0.89 and 0.93, respectively, which was higher than any other work that used a single US transducer element without using any ML algorithm. Kuru's first version of the hardware included only a single

transducer and suffered from the possible outcome that the transducer could miss the bladder completely, resulting in significant accuracy degradation. His second version of the hardware used five US transducers (including 1 transmitter and 4 receivers) in order to accommodate possible placement errors [23]. The information from the four receivers was first averaged before being processed for extracting the bladder volume. However, the new hardware still did not solve the problem that some of its receiving transducers could miss the bladder, reducing the number of effective transducers. In their latest study [24], Neural Networks (NN) were applied for processing and classifying data acquired from US transducers. The reported sensitivity and specificity values were raised to 0.99 and 0.995 with almost identical hardware as their previous versions.

Although various wearable US devices have been proposed over the past decades, there are still several unmet challenges that prevent US-based bladder sensors from mass usage. In this paper, several novel techniques have been proposed to address the existing challenges.

Challenge 1: Conventional methods for bladder volume estimation rely on some unrealistic hypotheses, such as bladder shape being generic and sensors always being placed at optimal locations. Such incorrect hypotheses can lead to significant errors at practical conditions.

Proposed Solution: ML methods which does not rely on any pre-determined hypothetical geometric bladder shape or any specific mathematical equations for calculating the volume are utilized to classify the acquired samples under different shape and placement conditions.

Challenge 2: Since US signals attenuate quickly in a human body, most existing US device use high-voltage (HV) pulses, e.g., greater than 100 V, to excite US transducers in order to obtain sufficiently high signal-to-noise ratio (SNR). However, HV pulses require expensive HV-compatible hardware, consume a significant amount of power, and are more likely to cause thermal and cavitation effects in a human body [25] when being compared with their low-voltage (LV) counterparts.

Proposed Solution: The US transducers in this work are excited by LV pulses to conserve power and improve biosafety. To maintain a high SNR, the LV US signal is coded at the transmitter and later decoded at the receiver using SNR enhancement techniques, such as sequence modulation and pulse compression.

Challenge 3: In many existing US-based bladder monitoring systems, it has been assumed that among all receiving transducers, the one that was earlier responsible for transmitting the US signals sees the strongest echoed signal. However, since the bladder surface is curved and prone to mirror reflection, the receiving transducer that sees the strongest echoed signal is not necessarily the transmitting transducer. The incorrect assumption can either put unnecessary burden to the readout circuits or lead to neglection of more important information from a nearby transducer.

Proposed Solution: Similar to the full matrix capture (FMC) method that has been widely adopted in non-destructive testing applications [26], the elements in a multi-dimensional transducer array can be formed into different transmitting-receiving combinations for capturing the echoes from an extensive range. For cost saving purpose, 1D array is preferable to 2D and 3D arrays.

Challenge 4: Given that the exact location of the biological bladder is not visually accessible from the abdominal surface, there is a risk of the scanning device being positioned too high, resulting in the bladder being missed, or positioned too low, causing echoed signals to originate from the pubic bone rather than the bladder. Trial-and-error-based placement is effectively a hit-and-miss process, significantly compromising user confidence in such a sensor device. Some other placement procedures involve some sophisticated protocols in finding the optimal location. It takes time for new users to familiarize themselves with complex placement procedures, leading to poor user experience.

Proposed Solution: We propose a simple way to place the transducer array, suitable for untrained users. It offers ample tolerance to displacement errors.

II. METHODS

A. TRANSDUCER ARRAY

A custom US transducer array has been utilized in this work. The 1D array consists of 11 square US transducer elements mounted on a double-sided flexible printed circuit (FPC) board (see Fig. 2(a)). Each element (width = length = 10 mm, thickness = 1 mm, pitch = 11 mm) is made of piezoelectric ceramic (PZT-5H) with silver-coated electrodes (thickness = 80 μm). The resonance frequency of these elements are 1.95 $\pm$ 0.16 MHz. In Fig. 2(a), from top to bottom, elements S1 to S10 are bladder detection sensors pubic bone. Fig. 2(b) shows that the transducer array can be easily curved to wrap around a cylinder with a 9-cm diameter. The center-to-center distance between S1 and S10 is 9.9 cm, greater than the maximum possible bladder height over the pubic bone of a typical 9-year-old child whose full bladder volume is approximately 300 ml. It ensures that even if the transducer array is misplaced from the ideal location by up to $\pm$4.5 mm, the bladder is still visible to all ten bladder detection sensors. A displacement tolerance of $\pm$4.5 mm is sufficient because of the additional US element for locating the pubic bone.

Although our US transducer is of narrow band whose $-$3dB bandwidth is only 17% of the center frequency, it offers relatively high electromechanical coupling factor (Kt = 0.58) and low unity cost (unit price $<$ 1 USD), especially when being compared with the high-profile US transducers used in diagnostic US imaging. Both the US transducers and their routings are placed on the top side while the bottom side of the FPC board works as a ground plane. For enhanced SNR, the routing tracks on the top side have been further covered by an additional electromagnetic shielding layer (thickness = 18 μm) to prevent the faint echoed signals from being

IEEE Journal of Translational Engineering in Health and Medicine

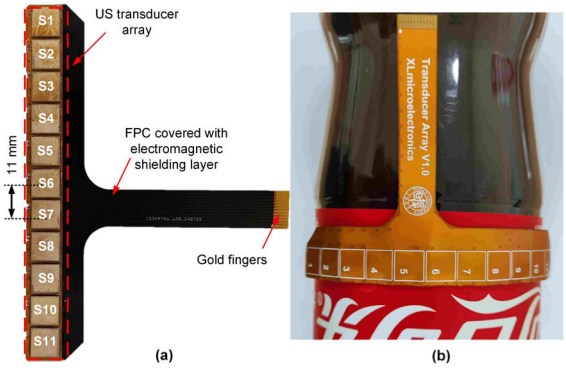

FIGURE 2. (a) The front view of the US transducer elements mounted on an FPC board. (b) The rear view of the FPC board.

contaminated by surrounding electromagnetic interferences. As the thickness of the FPC is merely 0.2 mm, it can be flexed to conform to the natural curvature of a user's abdomen.

B. HARDWARE

The functional block diagram of the proposed US system is shown in Fig. 3. It consists of a signal processing unit (in a computer), a pulse generator, a transmitting multiplexor (TX MUX), a receiving multiplexor (RX MUX), a T/R switch, an LV small-signal amplifier and an analog-to-digital converter (ADC). The hardware system works as follows:

i) A custom coded signal is first described in MATLAB in a PC before been transmitted to a low-voltage arbitrary waveform generator (DG2052, RIGOL®).

ii) A switch array with ultra-low on-resistance (ADG1412, ADI®) has been configured as a TX MUX so that the generated voltage pulses with $V_{pp} = 20$ V can be steered to the target US transducer element in the 1×11 array.

iii) Echoed signals are received by the receiving elements in the US transducer array and the signals are passed on for signal processing by the RX MUX. A T/R switch (MD0100, Microchip®) is usually placed between the RX MUX and the small-signal amplifier. This prevents large excitation pulses from coupling to the front-end of the amplifier, allowing only small echoed signals to be seen by the amplifier's input and maintaining the amplifier saturation free. The amplifier (AD8336, ADI®) consists of a low-noise front-end amplifier (LNA) and a programmable gain amplifier (PGA). An Arduino Due provides an analog voltage for setting the voltage gain of the PGA. The total gain is adjustable from 0 dB to 60 dB, depending on the amplitude of received echo signals. The amplified echo signals are then acquired by a high-speed data acquisition card (USB8916, ART Technology®). The digitized signals are sent to a PC for signal processing using the MATLAB's Filter Design and Analysis toolbox. A 60_{th}-order high-pass finite impulse response (FIR) filter has been constructed for removing low-frequency signals below 1.5 MHz. Both the TX and RX MUXs are controlled by the Arduino Due, as shown in Figs. 3 and 4. The control signals for TX MUX are also used for triggering the waveform generator while the control signals for RX MUX are used for triggering the data acquisition card. The acquired signals are transmitted to the computer via a USB interface which can be replaced by a wireless link in the future.

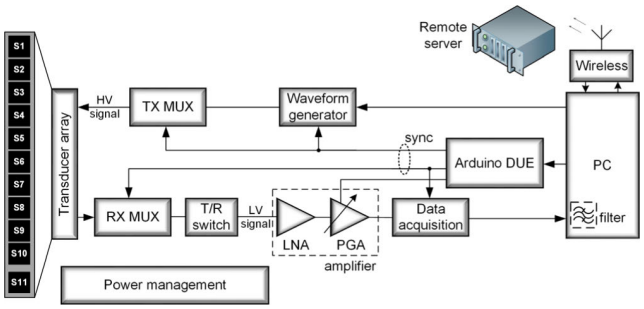

FIGURE 3. The functional block diagram of the proposed wearable US bladder monitoring system.

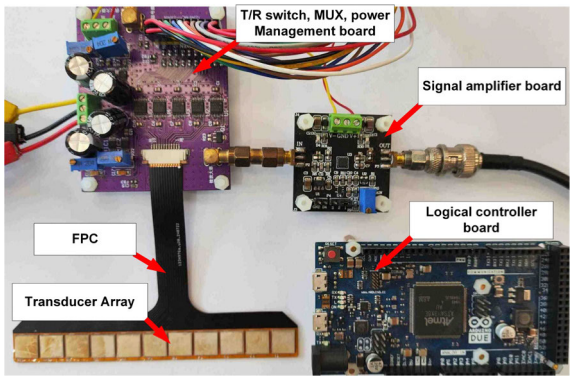

FIGURE 4. Customized circuits for transmitting, receiving, and logic control of US pulses.

C. CONTROL ALGORITHM

For an efficient FMC, a robust control algorithm is necessary for sequentially interrogating different US transducer elements. The proposed workflow of acquiring echoes from each individual element is shown in Fig. 5(a). Each data collection period has been divided into multiple measurement rounds. In the first round, the element S1 is responsible for transmitting while the elements S1 to S10 receive echoes. In the second round, the transmitting element changes to S2. According to the reciprocity principle, the S1 element does not need to receive any more, and the S2 to S10 elements are put into the receiving mode sequentially. The process is repeated until the element S10 completes transmitting the signal and receiving the echo. A total of 55 echo signals have been received during the ten different rounds. During the i_{th} round, elements are sequentially enabled for acquiring the echoes. Each receiving element is enabled for 4 ms and rests for 4 μs before the next element is enabled, as depicted in Fig. 5(b). Hence, the i_{th} round lasts for T (ms):

$$T = 4 \times (11 - i) + 0.004 \times (10 - i) \tag{4}$$

Within the 4 ms when a receiving element is enabled, the Tx broadcasts the coded signal (i.e., TX pulse) four times in 1 ms interval. Each corresponding echo has been captured and averaged for enhanced SNR. Due to the very short duration of the time frame, the bladder appears 'static' in bladder shape. The TX pulses and echo acquisition are synchronized by a trigger signal (see Fig. 5(b)). The excitation pulse lasts for 18 μs which is long enough to enclose the entire customized coded signal (see Section-D for further details). The duration of each echo acquisition, T_{acq}(s), should be long enough to capture the slowest echo. T_{acq}(s) is determined by the maximum scanning depth $D_{\max}$ (m) and the maximum gap $G_{\max}$ (m), which is the center-to-center distance between elements S1 and S10:

$$T_{\text{acq}} = \frac{D_{\max} + \sqrt{D_{\max}^2 + G_{\max}^2}}{c} \tag{5}$$

where $c = 1540$ m/s is the typical speed of acoustic signal in soft tissue. Assuming an ellipsoid-shaped bladder with a volume of 300 ml, the distance between the anterior and posterior walls may reach 10 cm, and with the addition of a distance of 4 cm from the anterior wall to the skin surface of abdomen, a representative distance between the skin surface of abdomen and the posterior wall is 14 cm. To accommodate possible variations among individual patients, we have designed a US system that is able to measure up to 18 cm away from the abdomen skin. While the $G_{\max}$ is 9.9 cm in the proposed 1D transducer array, $T_{\text{acq}} = 250$ μs is long enough for recording all possible echo signals reflected from the bladder. The 250-μs signal contains 10,000 samples in the time domain under 40Msps sampling rate.

The shortest distance from the abdomen skin to anterior bladder wall occurs when the bladder is full. In practice, this shortest distance is about 2cm to 4 cm varying in individuals, so the echo signal from a scanning depth less than the shortest distance bears no bladder-shape-related information. Hence, the first 0 to 3000 samples in raw signal can be discarded and the final length of raw echo signal is 7,000 samples in each channel.

D. US SIGNAL PROCESSING

In this work, the amplitude of excitation pulses is limited to ± 10 V which is lower than what was reported in similar works. Low-voltage excitation pulses lead to smaller echoed signals. In order to enhance the SNR at the US receivers, coded excitation pulses, such as the ones using the Barker code, Golay code, and chirp code have been used [27]. We opt for the Barker code because the amplitude of the side lobes for Barker coding is smaller than those of other codes of the same length [28]. However, short Barker code is not compatible with the low-cost transducer used in this work only has 17% fractional bandwidth and is not suitable for short-pulse excitation because the bandwidth of the excitation signals is much larger than that of the transducer itself. To alleviate the bandwidth problem and to concentrate the majority of signal energy within the limited bandwidth of the

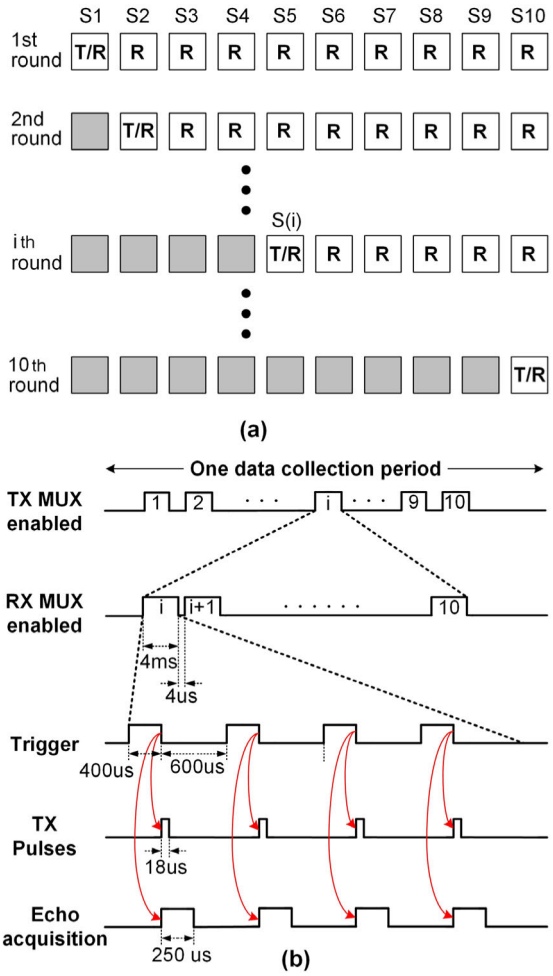

FIGURE 5. (a) The working roles of US elements in different rounds. Elements in gray color are inactive; (b) Time sequence for transmitting and receiving US pulses.

transducer, the total length of the Barker code is expanded by modulating a 5-bit Barker code $B(5) = \{1, 1, 1, -1, 1\}$ where $\{1\}$ and $\{-1\}$ in the code sequence represent 0° and 180° phase signals, respectively, by $S(7) = \{1, 1, 1, 1, 1, 1, 1\}$ which is a 7-cycle continuous sine wave. By choosing the frequency of the sine wave to be 1.95 MHz which is the same as the resonant frequency of the transducer, we are able to confine most of the energy in the Barker code within the limited bandwidth of the chosen transducer. The modulation process is the Kronecker product of the Barker code and base sequence [29], that can be described by (6):

$$X(n \times m) = B(n) \otimes S(m) \tag{6}$$

where the $B(n)$ is Barker code sequence, $S(m)$ is base sequence, and $X(n \times m)$ is the modulated sequence. The original 5-bit Barker code is shown in Fig. 6(a) while Fig. 6(b) shows the output waveform after the 5-bit Barker code is modulated with a 7-bit base sequence. Fig. 6(c) shows the frequency spectrum of the Barker code with and without modulation. The original 5-bit Barker code (red dash line)

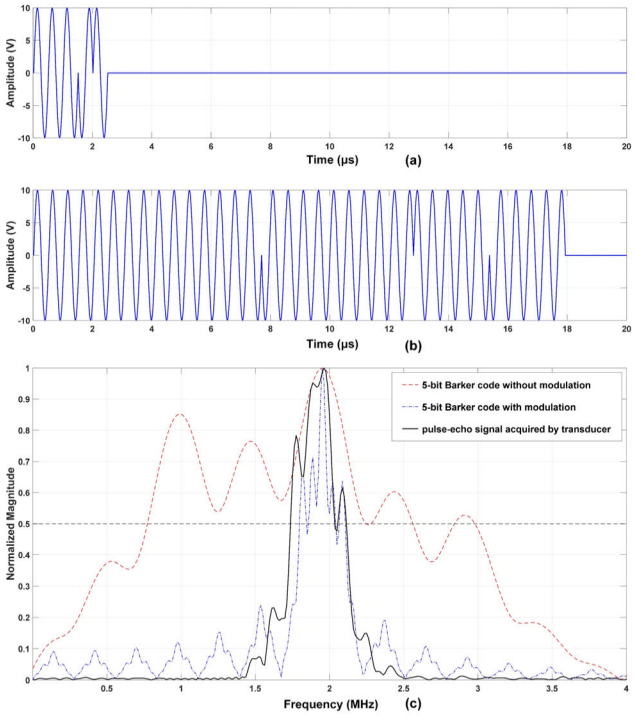

FIGURE 6. (a) The output waveform of a 5-bit Barker code without modulation; (b) The output waveform of a 5-bit Barker code modulated with a 7-bit base sequence; (c) The frequency spectrum of the Barker codes with and without modulation, and the pulse-echo signal acquired by the transducer.

without modulation has much wider bandwidth than that of the practical transducer (black solid line). Hence the transducer is effectively a band-pass filter and causes significant energy loss of the transmitted signal. However, the signal bandwidth of the modulated Barker code (blue dash-dot line) fits well within the narrow bandwidth of the transducer.

The decoding process of received echo is filtered by a matched filter $X(-n)$ which is in the form of time-reversed copy of $X(n)$ in the time domain. The process of matched filter output compresses the long pulse into a much shorter duration pulse is called pulse compression. In this technique, the coded excitation with long pulse duration is expected to increase the SNR of the echo. The SNR at the US receiver's input is defined as [27]:

$$\mathrm{SNR} = 10 \cdot \log_{10} \frac{P_{\mathrm{signal}}}{P_{\mathrm{noise}}} = 10 \cdot \log_{10} \left(\frac{A^2_{\mathrm{signal,\,RMS}}}{A^2_{\mathrm{noise,RMS}}} \right) \quad (7)$$

where the P_{signal} and P_{noise} are the power of signal and noise, respectively. $A_{\mathrm{signal,RMS}}$ and $A_{\mathrm{noise,RMS}}$ are the root-mean-square amplitude of the signal and noise, respectively.

Theoretically, the SNR gain of a decoded echo is the SNR ratio of the decoded echo to the original echo, which related to the total number of chips in the coded pulse [27] and can be calculated by:

$$SNR_{\mathrm{gain}} = 10 \cdot \log (N \cdot M) \quad (8)$$

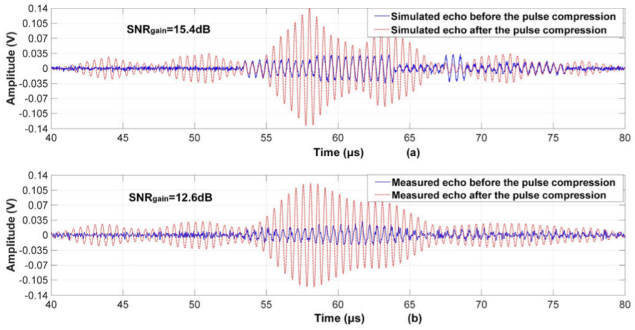

FIGURE 7. (a) Simulated echo before (blue solid line) and after (red dotted line) the pulse compression; (b) Measured echo before (blue solid line) and after (red dotted line) the pulse compression. The SNR is enhanced by using the technique of pulse compression.

where the N and M are the length of the Barker code and base sequence, respectively. For $N = 5, M = 7$, the theoretical gain using the coded signal is 15.4 dB without increasing the excitation voltage. The waveforms in Fig. 7 show the SNR is enhanced by the pulse compression. It also can be seen that the measured echo's SNR gain (see Fig. 7(b)) obtained using pulse compression technique is 12.6 dB, which is 2.8 dB less than the SNR gain (15.4 dB) of simulated echo (see Fig. 7(a)). The reason for the reduced gain is that due to the non-linear attenuation of the transmission medium, the waveform of practical echo does not completely match the ideal Barker code waveform, thus affecting the effectiveness of pulse compression. It is worth noting that the echo after the pulse compression consists of two peaks in the main lobe. In our experimental setup, the transducer array was attached to the outside wall of the water tank. When the sound wave passes through the water tank's wall, it is partially reflected at the solid-liquid interface and re-reflected by the surface of transducer in a short time. The time interval between the two peaks equals to two times the thickness of the tank wall (5.5 mm) divided by the acoustic speed in acrylic (2650 m/s). This is the reason why the two peaks appear in the main lobe. Comparing the waveforms before and after pulse compression, the use of coded excitation and pulse compression technique can significantly improve the SNR of echoes, which is crucial for subsequent signal processing and classification.

E. DATA ANALYSIS IN THE TIME-FREQUENCY DOMAIN

Apart from echo variations in the time domain, the accumulation of urine in bladder also produces a nonlinear effect leading to variations in the frequency domain [22]. Hence, analyzing the echo signals in both the time and frequency domains can potentially enhance the prediction accuracy. The short-time Fourier transform (STFT) is a common method for analyzing how the frequency contents of a signal changes over time. The process of STFT is to divide a raw signal into many small segments by a sliding window and to perform discrete Fourier transform on each individual segment. The

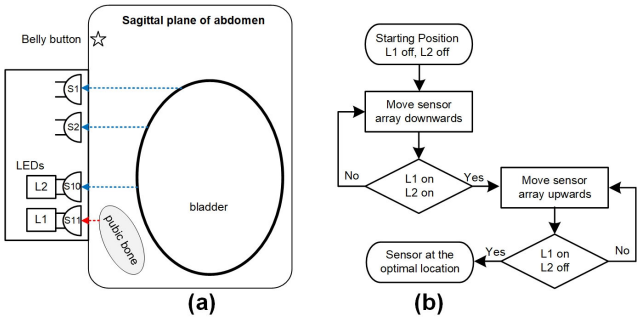

FIGURE 8. **(a) Diagram of the device positioning (from the view of sagittal plane); (b) Workflow of positioning the device by users.**

outcome of the STFT is given as (9) [30]:

$$X(m,n) = \sum_{k=-\infty}^{+\infty} x(k)\, w(k-n)\, e^{-j\frac{2\pi}{N}mk} \tag{9}$$

where $x(k)$ is the echo signal in the time domain, $X(m,n)$ is a function of both time and frequency, $w(k)$ is the transfer function of the sliding window, n represents the time-shift parameter of the window, m is the frequency index, and N is the total length of signal. When each segment is non-overlapped, there may be abrupt changes between successive windows, causing undesirable artifacts. Overlapping windows can mitigate this issue by smoothing the transitions between successive segments [31]. The length of the window is determined by trading-off the time resolution and frequency resolution according to the Heisenberg's uncertainty principle. In this work, the acquired signal in each US channel is divided into segments by STFT using a Hamming window. Each Hamming window contains 128 samples, 50 of which were overlapped with the next window.

F. ASSISTANT POSITIONING

In practice, if the US sensor is placed too low, the bladder will not be visible to the lower part of the transducer array as only the echoes from the pubic bone, not the bladder, are detected. The conventional placement method tends to be empirical. For instance, it is recommended to place the US sensor 5 cm above the pubic bone. This method can avoid placing the US transducer over the pubic bone. But if the US sensor is placed too high, it can also result in a reduction in the number of effective US elements.

We propose an assistant positioning method by using the lowest transducer element, i.e., S11 in the custom array, for aligning with the pubic bone (see Fig. 8(a)). Hence the positions of S1 to S10 are higher than the pubic bone.

Our method utilizes the fact that the typical acoustic impedance of a pubic bone ($Z = 7.8$ MRayl) is significantly different from those of the surrounding soft tissues ($Z = 1.6$ MRayl), so a US beam is repeatedly reflected back and forth between the pubic bone and the transducer, producing typical reverberation artifacts in B-mode images [32]. Such an effect also appears in A-mode US, as 2 or 3 high-amplitude wave crests are evident in the A-mode echoes reflected from pubic bone. The time intervals between adjacent wave crests are determined by the TOF for an ultrasound to travel a round trip between the S11 and pubic bone. In contrast, the amplitude of echoes from the bladder are much lower than that of the pubic echo. The high-amplitude wave crests are used as a simple biomarker for identifying the pubic bone.

The protocol for placing the custom transducer array is as follows:

Firstly, the belly button, a prominent landmark on the abdomen, is used as a starting position for placing the transducer array. The linear array is placed on a subject's abdomen and the mid-line of the linear sensor array matches the lineae mediana anterior. Then, the subject needs to align the 3rd lowest US element from the bottom with his/her navel. At this moment, both the LEDs, L1 and L2, are off, indicating US elements S10 and S11 are both above the pubic bone. Secondly, the sensor array is gradually moving downwards towards the subject's feet. The movement ceases when both L1 and L2 are turned on. Thirdly, the linear array is moving in the opposite direction (i.e., towards the subject's head) until L2 starts to turn off while L1 remains on. The workflow for positioning is shown in Fig. 8(b).

G. MACHINE LEARNING

1) PCA-BASED FEATURE EXTRACTION

The raw data captured by each individual receiving US element contains $K1$ byte:

$$K1 = a1 \times b1 \times c1 \tag{10}$$

where $a1 = 7000$ is the number of data samples, $b1 = 55$ is the number of transceiver channels, $c1 = 8$ is the data length for each recorded data point.

After the STFT, the total data length has been reduced to:

$$K2 = a2 \times b2 \times c2 \tag{11}$$

where $a2 = 6400$, $b2 = 55$, $c2 = 8$. $K2$ is lower than $K1$, but still too much. Hence, feature extraction can significantly reduce the number of data dimensions, avoiding data overflow. Also, it can extract the essential characteristics from the raw data. We extract features from the recorded data before training models. In this work, the principal component analysis (PCA) is applied to combine highly correlated high dimension variables in raw signals into less dimensional variable with low linear relativity and minimal information loss. As the bladder size varies against time, for the same US element, the amplitude of the echoed signal may vary significantly over time. Thus, it is necessary to perform standardization before PCA. The samples are standardized prior to PCA. The procedure of standardization can be described as:

$$Z = \frac{x - \mu}{\sigma} \tag{12}$$

where the x is the input data, μ is the mean of the input data, and σ is the standard deviation of the input data.

To achieve good dimensional reduction without significantly compromising the accuracy of the original dataset, the principal components that account for more than 90% of the data variation have been selected in this work.

2) CLASSIFICATION

Artificial intelligence (AI) is a powerful technology used for tasks such as facial and speech recognition, real-time translation, and complex decision-making. In many AI approaches, ML methods are particularly effective at deriving useful insights from limited datasets and are widely adopted for biomedical signal analysis and disease diagnosis, especially suitable for deployment in wearable medical devices. For example, support vector machines (SVM) and artificial neural networks (ANN) have been used for predicting hematic parameters of blood [33]. SVM, K-nearest neighbor (KNN) and Logistic regression (LR) have been applied for diagnosing the Parkinson's Disease [35]. SVM and random forest (RF) have been utilized for bladder monitoring [36]. Biomedical signals are often multi-dimensional, non-linear and sensitive to noise. ML excels at identifying relevant characteristics from raw signals and processing complex and noisy biomedical signals. ML is also not new to bladder monitoring. Among various ML methods for bladder monitoring, KNN [34], [45] and SVM [36], [45] are two of the most frequently used approaches because they usually require a shorter training time for a small dataset and are less prone to overfitting. Neural network is also popular as it often achieves good classification performance [24], but it requires a large amount of data in order to avoid overfitting, and both training and testing demand significant computational resources, which limits their application in wearable devices. In addition, sparse coding (SC), which is a well-known unsupervised dictionary learning method [37], has recently emerged as a useful tool for efficiently representing high-dimensional data. Although SC has previously been applied to various tasks, such as biometrics recognition [47], diagnosis of nervous system disorders [48], to the authors' best knowledge, this is the first time, SC has been utilized for bladder monitoring application. In Section IV, we compare classification performance under different ML algorithms.

SC can be used to find a set of over-complete sparse basis vectors $\boldsymbol{\phi}_i$ to represent the input vector $\boldsymbol{X}$ more efficiently, as describe in (13):

$$\boldsymbol{X} \triangleq \sum_{i=1}^{k} \boldsymbol{\alpha}_i \boldsymbol{\phi}_i \tag{13}$$

where the $\boldsymbol{\alpha}_i$ are the sparse coefficient matrix that should have very few non-zero elements. To find the sparsest solution, the sparse coding optimization problem can be written as:

$$\underset{\alpha}{argmin}[(\frac{1}{2}\|\boldsymbol{X} - \boldsymbol{\phi}\boldsymbol{\alpha}\|_2^2) + \lambda \|\boldsymbol{\alpha}\|_1] \tag{14}$$

where the first term represents the reconstruction error between the original data and the linear combination of dictionary elements and the second term is L1 norm of the coefficient matrix, encouraging sparsity. λ is a controller that dictates the optimal trade-off between the reconstruction accuracy and sparsity. The optimization process aims to find the coefficient matrix that minimizes the reconstruction error while promoting a sparse representation. SC has the advantage of learning the essential features inherent to the data, leading to a significant reduction in redundant information and noise, thereby enhancing the model's accuracy and generalization capability. Additionally, it operates as an unsupervised learning algorithm, eliminating the need for manual data labeling, and can efficiently leverage a vast amount of unlabeled data for learning, eliminating the need for laborious manual feature extraction.

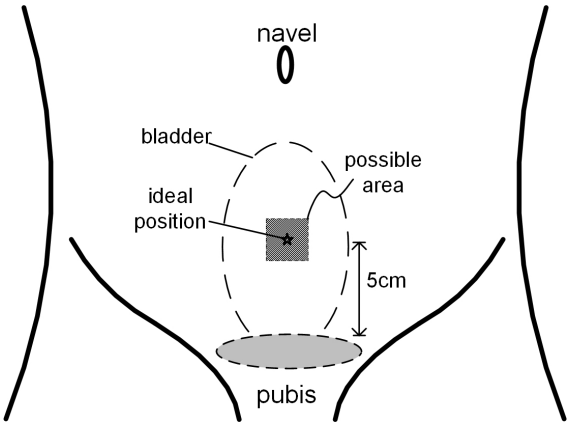

FIGURE 9. The star is the ideal position for placing US transducer. In this work, the possible shifting area is 10 mm × 10 mm square area.

3) PARAMETER OPTIMIZATION

KNN has no explicit training phase, but simply stores the entire training dataset. The value of k (i.e., the number of nearest neighbors) has been optimized through cross-validation on the training dataset. The training dataset for SVM consists of feature vectors and corresponding class labels. In a training process, a kernel function (e.g., linear, polynomial, or radial basis function (RBF)) is chosen to transform the data into a higher-dimensional space where it is more likely to be linearly separable. The penalty parameter in SVM is also essential for managing the trade-off between margin maximization and misclassification minimization. A dictionary for SC is initialized by randomly combining the input vectors in the training process. The regularization parameter is a hyperparameter that needs to be carefully tuned to find the optimal balance between sparsity and reconstruction accuracy during training.

We apply K-fold cross validation and grid search methods to optimize the hyperparameters used in KNN, SVM and SC for high performance and generalize better to new data. Firstly, we defined a grid of hyperparameters (e.g., number of neighbors, kernel type and regularization parameter) to explore. Then evaluated each combination of hyperparameters using 5-fold cross-validation. Finally, we found the

combination of hyperparameters that yields the best cross-validation performance.

4) USEFULNESS OF ML

Using the proposed assistant positioning method, it is guaranteed that the ideal location for placing the sensor can be found without missing the bladder. However, even with assistant positioning, the practical position may vary from the ideal position, due to many unavoidable reasons, so ML can further solve this problem.

According to a study on the changes of bladder shape during filling [38], it was found that the bottom of bladder hardly moves in the entire filling process and that the maximum expansion of bladder walls occurs in the cranial direction.

By using the assistant positioning method, the transducer array can be placed in the position above the pubic bone (except for the element dedicated to sense the pubic bone), with its center, i.e., the mid-point of element S5 and element S6 locates approximately 5 cm above the pubic bone, which is consistent with the position described in the literature for placing single US transducer [22]. We can regard the position as an ideal position for placement, as depicted in Fig. 9. In this work, we assume that the center of the transducer array would be misplaced from the ideal position in the up, down, left and right directions. In other words, the possible shifting area is a square area of 10 mm × 10 mm. During the period of sample acquisition for training, an optimal method involving incremental position movement (2 mm per step) and capturing the echo signals from different volume intervals (2 ml, 4 ml, 6 ml, or 8 ml), is used to construct the training dataset. Firstly, we search the algorithm that achieves the best classification performance, within the region within an area of 10 mm ×10 mm. Next, we increase the movement step, while keeping other conditions constant, this process aims to find the balance between good classification performance and short training time.

III. VALIDATION EXPERIMENTAL SETUP

The proposed prototype device and machine-learning algorithm have been validated on a latex balloon placed in an acrylic water tank, as shown in Fig. 10(a). The inlet of the balloon is held constant by a clamp. The thickness of the water tank wall is 5.5 mm. To simulate the bladder filling process, water is slowly injected into the balloon from a water bottle by a programmable laboratory peristaltic pump (KE-300EL, Jieheng®). The volume of injected water is calculated by measuring the weight loss from the water bottle by a digital electronic balance (Cmq-196, CGOLDENWALL®) which has a measurement resolution of 0.1 g. The transducer array is mounted on the outside of the tank wall facing the balloon. US coupling gel is applied between the transducer surface and the tank wall to make sure that there is an efficient pathway for US propagation. The residual air inside the balloon before the water injection can be removed by running the water pump in the extraction mode first before pumping water into the balloon.

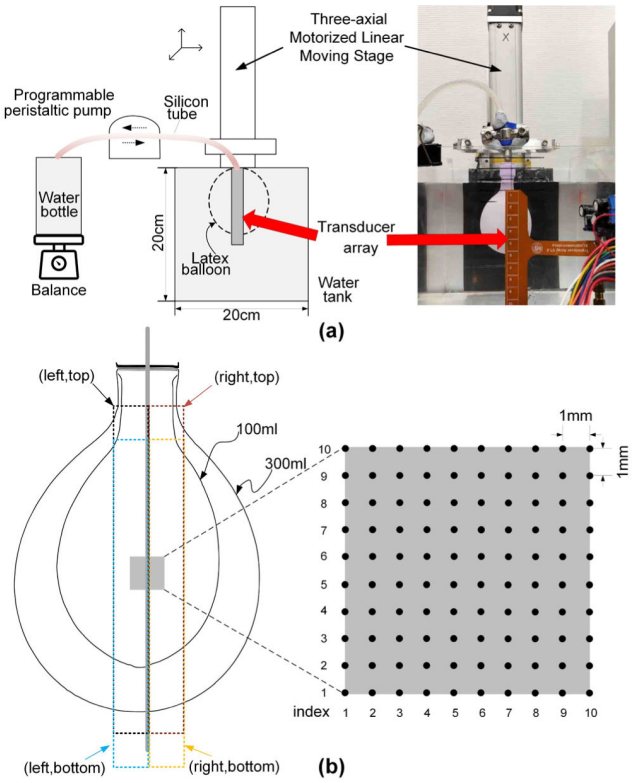

FIGURE 10. (a) The diagram of experimental setup and its real photo; (b) In this work, the balloon volume changes from 100 ml to 300 ml, and the position varies 100 times with 1 mm step.

When a bladder is empty or at low volume, the majority of the bladder is hidden behind the pubic bone, making the detection difficult [39]. However, low volume is of no interest to the proposed bladder monitoring application intended for patients suffering from nocturnal enuresis. Hence, the minimum volume to be classified is set at 100 ml in this experiment. Whether a bladder volume is less than 100 ml or not can easily be determined by the absence of echoes from bladder. The maximum volume in this experiment depends on the expected bladder capacity (EBC) in children, which varies with age and can be estimated by an empirical formula [40]:

$$\text{EBC (ml)} = 30 \times \text{Age} + 30 \tag{15}$$

In this work, the maximum volume for trigger an alarm is chosen as 300 ml that can almost cover all 9-year-old children and younger. In this experimental setup, 1 ml of water is injected into the tank from the water bottle at a time, and the balloon's volume varies from 100 ml to 300 ml. Therefore 201 different balloon volumes have been created.

To simulate the misplacement of the transducer array, we alter the relative location of the transducer array to the balloon. This can be achieved either by making the balloon static and moving the transducer array around a central point, or by making the transducer array static and moving the balloon. We opt for the latter approach as constantly moving the transducer array may compromise the efficacy of the

IEEE Journal of Translational Engineering in Health and Medicine

coupling at the transducer-tank interface. The movement of balloon was driven by a three-axis motorized moving stage (FG50XYZ, TNE®) which offers an absolute positioning accuracy of 20 μm and a repeated positioning accuracy of 10 μm. The moving stage is programmed to cover an area of 10 mm (in the x direction) $\times$ 10 mm (in the y direction) with a step size of 1 mm. Hence the moving stage created 100 different relative locations between the sensor array and the balloon. The upper-right, upper-left, down-right and down-left positions of transducer related to balloon is shown in Fig. 10(b). The total sets consist of 100 $\times$ 201 sampled data.

A. THE CLASSES OF VOLUME

The urgent status for voiding can be divided into several statuses according to the bladder volume that allows users to set different pre-voiding threshold according to their individual conditions. The gap volume of different threshold is decided by the filling rate of urine. Assuming a child with 25 kg weight and high filling rate 2.0 ml/(kg·h) [41], it takes about one hour to increase 50 ml urine in the bladder at night. The period is long enough for parents to wake their kids up before voluntary voiding. Therefore, the 50 ml gap between different alarm thresholds is reasonable.

Although some children produce urine less than the EBC during the night, based on the fact that most children urinate when their bladder capacity is close to the EBC, to simplify the analysis we labeled 100 ml to 249 ml into 'low-volume' samples while the others are 'high-volume'.

B. TEST CASES (TC)

Three different test cases have been formed using different training sets and test sets to simulate different scenarios. Each set is derived from the total set based on different volume step (VS) and position step (PS).

1) TC1 (Single-location training, same location testing):

Hypothesis: the transducer array can be placed at the desirable position. In other words, the array location (coordinates [5, 5] in Fig. 10(b)) during testing is the same as that during training.

Experimental conditions: In this case, different volumes (VS = 2 ml) in training sets and all the volumes (VS = 1 ml) in test sets, which means only a half of test sets are observed in training sets.

2) TC2 (Single-location training, random placement for testing):

In practice, the placement of transducer array may shift from the ideal position.

Experimental conditions: In this case, the position of training sets still come from the ideal position and different volumes (VS = 2 ml). But the test sets consist of all positions (PS = 1 mm) and all volumes (VS = 1 ml). Almost all of the test sets never seen in training sets, except for some data from the ideal position.

TABLE 1. Summary of classification results.

Test case	ML method	VS	PS	Precision	Recall
TC1	KNN	2	0	0.92±0.08	0.81±0.09
	SVM	2	0	0.95±0.03	0.89±0.05
	SC	2	0	0.96±0.02	0.96±0.02
TC2	KNN	2	0	0.24±0.36	0.25±0.36
	SVM	2	0	0.17±0.33	0.21±0.37
	SC	2	0	0.40±0.28	0.51±0.34
TC3	KNN	2	2	0.89±0.18	0.80±0.24
	SVM	2	2	0.94±0.19	0.82±0.26
	SC	2	2	0.98±0.07	0.94±0.08
TC4	SC	2	2	0.98±0.07	0.94±0.08
			3	0.90±0.16	0.97±0.07
			4	0.85±0.19	0.93±0.11
		4	2	0.96±0.08	0.96±0.07
			3	0.90±0.14	0.96±0.08
			4	0.85±0.20	0.88±0.14
		6	2	0.96±0.08	0.95±0.10
			3	0.87±0.17	0.94±0.10
			4	0.78±0.22	0.90±0.13
		8	2	0.95±0.07	0.92±0.08
			3	0.83±0.18	0.92±0.12
			4	0.85±0.20	0.82±0.18

3) TC3 (Multi-location training, random placement for testing, fixed PS and VS):

To overcome the practical limitation on sensor misplacement, a multi-location training strategy has been adopted in this work. Firstly, training sets are composed of different position steps (PS = 2 mm) and different volume steps (VS = 2 ml). The three classification methods from Section-G have been used for classifying the test sets in all positions.

4) TC4 (Multi-location training, random placement for testing, variable PS and VS):

Experimental conditions: different PS (values 2 mm, 3 mm and 4 mm) and different VS (values 2 ml, 4 ml, 6 ml and 8 ml) are applied in the training sets. The test sets are the same as TC2. The larger PS and larger VS mean less samples in the training process, which helps to reduce the training time, and less US dosage in the training process, which is desirable from the health and safety perspective.

IV. RESULTS

Although accuracy is the most direct and widely used metric for evaluating classification models, it requires a balanced number of samples in each class.

$$\text{accuracy} = \frac{\text{TP} + \text{TN}}{\text{TP} + \text{FP} + \text{TN} + \text{FN}} \tag{16}$$

where the TP is true positive, FN is false negative, FP is false positive and TN is true negative. For our particular bladder monitoring application, the number of samples in the low-volume class is much higher than that in the high-volume class. In this work, we have chosen precision and recall as the performance indicators for classification. Precision and recall

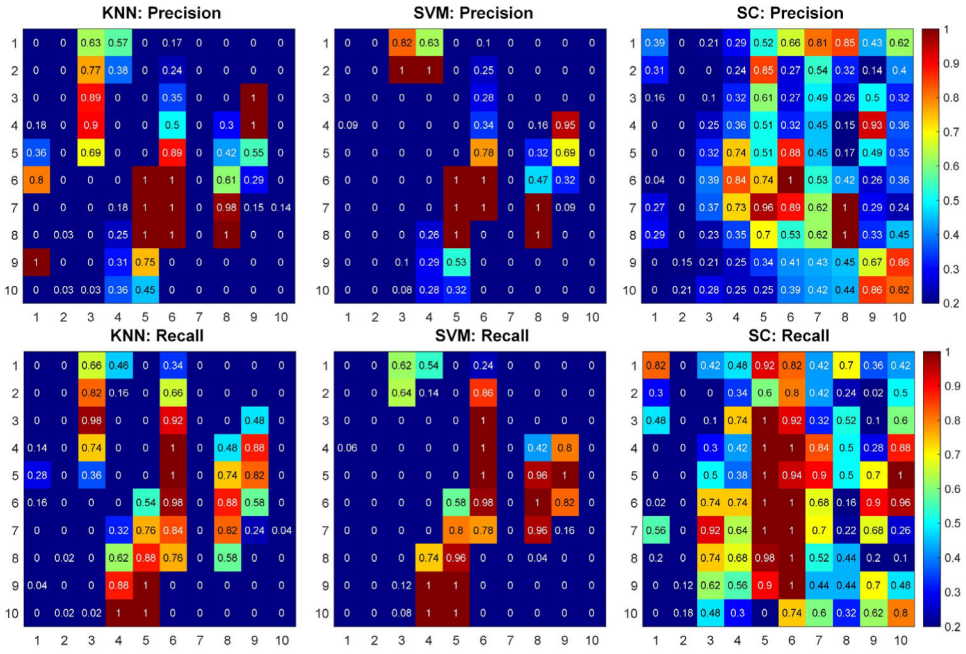

FIGURE 11. Classification results of TC2.

are defined as:

$$\text{precision} = \frac{\text{TP}}{\text{TP} + \text{FP}} \tag{17}$$

$$\text{recall} = \frac{\text{TP}}{\text{TP} + \text{FN}} \tag{18}$$

TC1 has been performed 10 times. During each time, the training process has gone through a 5-fold cross validation under different classification methods. TABLE 1 shows the average results after 10 trials. In general, all three classification methods showed good capability in classifying different volume samples as the mean precision and mean recall results for all three classification methods were close to or above 0.90. Specifically, precisions ranked from low to high are from KNN (0.916 $\pm$ 0.08), SVM (0.946 $\pm$ 0.03) and SC (0.957 $\pm$ 0.02). Recalls ranked from low to high are from KNN (0.814 $\pm$ 0.09), SVM (0.894 $\pm$ 0.05) and SC (0.958 $\pm$ 0.02). In addition, SC also shows the best stability performance among the three methods, as being evident from its small standard deviation. The best classification performance of SC is based on slightly longer execution time: 281 ms (SC) vs. 261 ms (KNN) vs. 220 ms (SVM).

Fig. 11 shows that the classification results dramatically deteriorate when the position of the test sets (randomly chosen from the 10 mm 10 mm area) is different from the position of the training sets. The precision and recall reduce to below 0.5 for most position cases which are 2 mm or more away from the ideal position, and the statistical results in different positions are shown in TABLE 1. Such low precision and recall values are unacceptable for any practical use. It indicates the US system is extremely sensitive to misplacement of the transducer array. In addition, the performance degradation is more pronounced when the transducer array is moved along the horizontal direction than that along the vertical direction. This is due to the vertical configuration of individual elements in the transducer array.

The precision and recall for almost all positions in TC3 (i.e., using multiple positions training), shows in Fig. 12, are higher than those in TC2. SC offers a superior performance to KNN and SVM. By using the SC method, precision at 97% of the positions are higher than 0.75, while recall at 98% of the positions is higher than 0.75.

In TC4, using the SC approach, the classification results obtained at VS = 6 ml were comparable to those obtained at VS = 2 ml when PS = 2 mm. The result matrix is shown in Fig. 13. For a given PS = 2 mm, reducing VS from 6 ml to 2 ml leads to only 1.3% increase in the average precision; however, the acquisition frequency needs to be tripled, which is burdensome to user. For a given VS = 2 ml, by increasing PS from 2 mm to 3 mm, the average precision decreased from 0.975 to 0.897. The rate of reduction was 8%. This result corresponds with the results for TC2, in which the system is very sensitive to displacement. If both PS and VS can be set freely, the average precision difference between (PS = 2 mm, VS = 2 ml) and (PS = 3 mm, VS = 6 ml) is only 5% in the center of the smaller area (6 mm10 mm), where precision $\geq$ 0.75 occurs at 98% of the positions, and recall $\geq$ 0.75 occurs at 98% of the positions. Both the average precision and recall are above 0.85 in all positions from the TABLE 1, shows the combination (PS = 3 mm, VS = 6 ml) is a good choice for training.

V. DISCUSSION

The issue on sensor misplacement is usually neglected by conventional ultrasound sensor system for bladder monitoring. The high classification accuracy of conventional

IEEE Journal of Translational Engineering in Health and Medicine

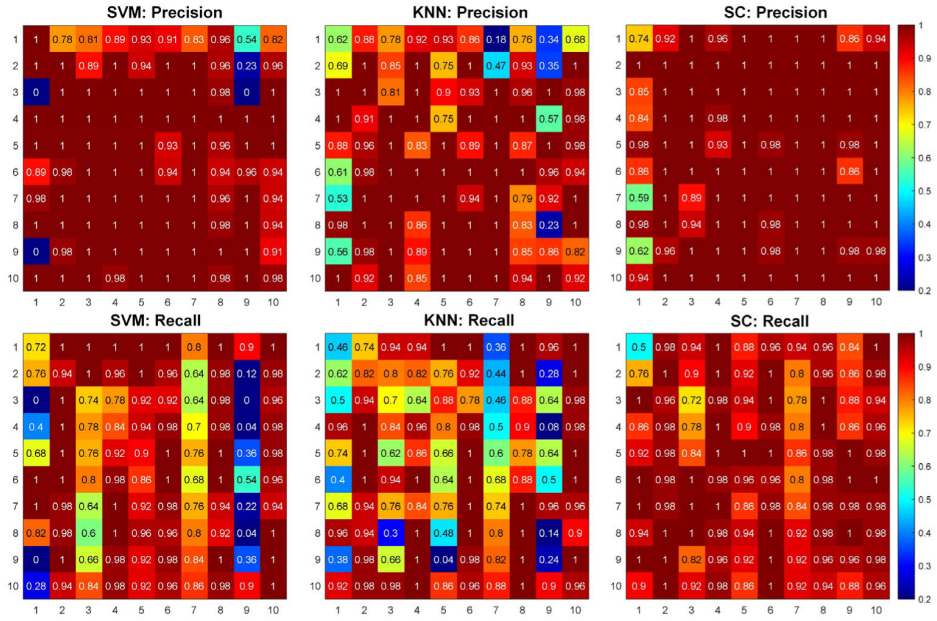

FIGURE 12. Classification results of TC3.

systems relies on two unrealistic hypotheses: i) The sensor can be placed at the ideal position which offers the best sensitivity and accuracy, ii) The sensor location during practical usage is the same as the location during the training process. In contrast, we acknowledge the fact that not everyone can place the sensor at the ideal location and even for a trained user, he/she cannot always place the sensor at the ideal location. We propose a robust system that offers ample tolerance to possible sensor misplacement. Insensitivity to sensor placement has been achieved by two novel techniques: i) a guidance protocol for locating the pubic bone. By doing so, the sensor may not be placed at the ideal location, but it will be within a controlled range not far from the ideal location; ii) the multi-position training strategy ensures the sensor system can offer reasonably high classification accuracy as long as the sensor is within the controlled range.

From the TABLE 2, we can see the differences between our work and other similar works. Among all the works, the amplitude of the excitation signal we adopted is the smallest. Similarly using the ML algorithm for classification, our classification performance is higher than that work [22], demonstrating that the transducer array can capture more valuable echoes than single element. In [24], they achieved higher classification performance than ours, but their high classification was built upon wide-bandwidth transducers and computation-heavy neural networks. The former makes transmitting frequency-modulated signals easy at the cost of high-end US transducer while the latter consumes significant amount of power. In [42], researchers implemented US imaging patches that can accurately estimate bladder volume, but for the application of pre-voiding alarm, simple classification of different bladder filling levels is sufficient. The hardware system required to generate US images is quite complex and expensive. In comparison, our approach is more cost-effective.

The purpose of this work is to develop a bedwetting alarm device suitable for home usage. Hence, we put safety and usability as our first priority. A lower excitation voltage results in a lower acoustic pressure. Since acoustic intensity is proportional to the square of acoustic pressure, using LV pulses means that the acoustic intensity produced for detecting bladder is far below than the Food and Drug Administration (FDA)'s safety limit of 720 mW/cm^2. Even with prolonged operation, the acoustic energy produced by the system will not generate heating or cavitation effects that could potentially harm the human body. The proposed device is well-suited for long-term wearable usage. To address the inevitable transducer misplacement issue during practical usage, we have introduced sparse coding and a multi-position training strategy, which significantly improve the classification performance.

VI. FUTURE WORK

In clinical applications, coupling gel is another challenge for wearable US devices. Applying coupling gel is a tedious process, it may get dry, compromising the signal quality. Most of engineering papers [14], [15], [16], [17], [18], [19], [20], [21], [22], [23], [24] on bladder monitoring still rely on the standard coupling gel to eliminate air gaps and ensure that sound waves are effectively transmitted from the probe into the body. It is a well explored research direction for forming a better contacting interface between transducer and skin, either by a better gel [43], [46] or no-gel [42], [44]. In the future clinical trials, we will consider using some special US coupling agent (such as hydrogel-elastomer hybrid gel and non-Newtonian fluid coupling media) that are biocompatible, have desired acoustic impedance, and prevent the transducer array from being detached from skin after long-term usage.

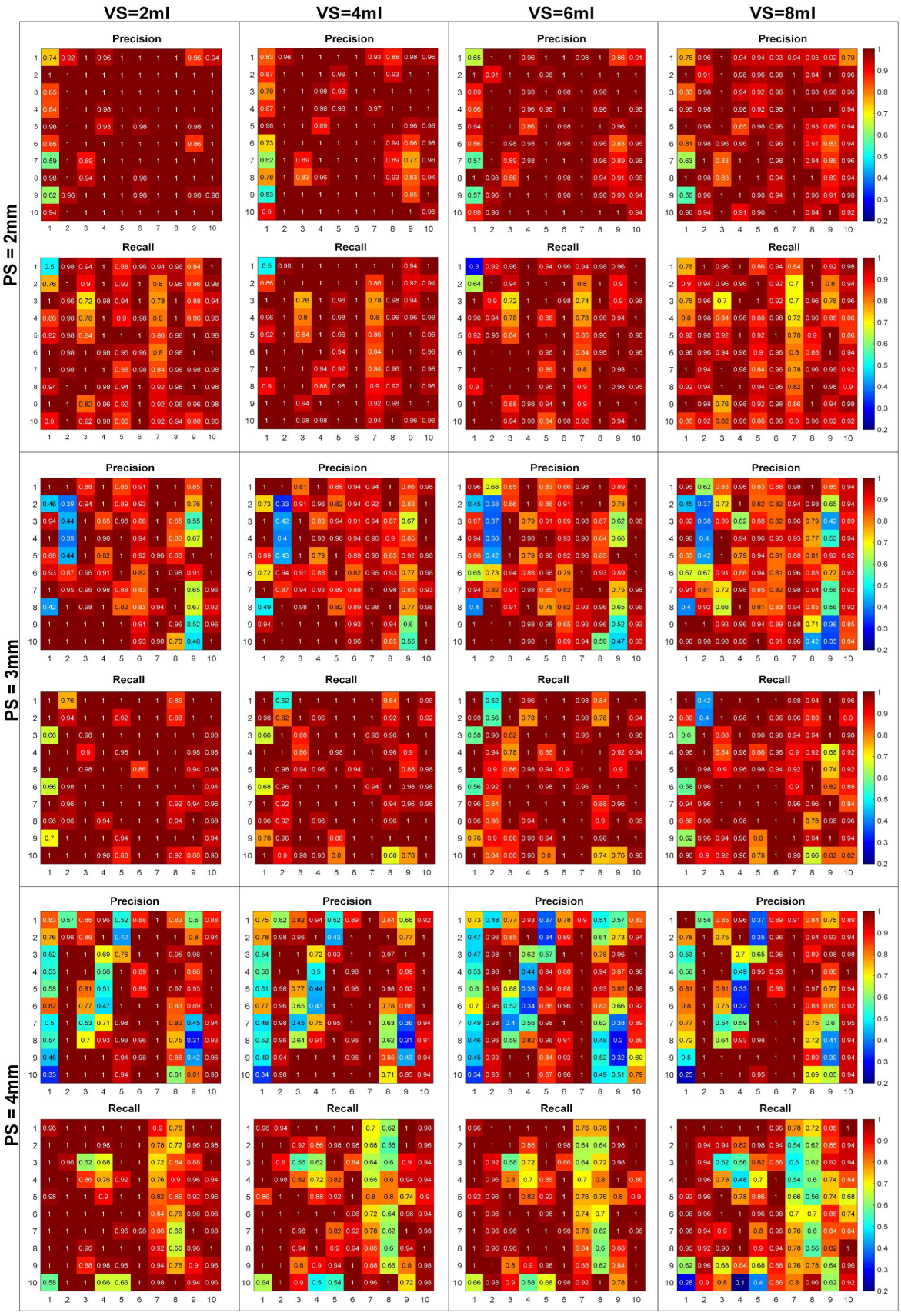

FIGURE 13. Classification results of TC4.

TABLE 2. Performance summary and comparison to prior arts.

	Sensors 2021 [20]	Med. Biol. Eng. Comput. 2019 [22]	IEEE J. Transl. Eng. Health Med. 2024 [24]	Nat. Electron. 2024 [42]	IEEE Sens. J. 2024 [44]	Our work
Number of US elements	5×5 2D array	1	2×2+1[Δ] 2D array	64×5 2D array	4×4 2D array	10+1 [&] 1D linear array
Tx and Rx configuration	Each element is sequentially activated. All US elements are transceivers.	Each element is sequentially activated. All US elements are transceivers.	All are simultaneously activated. Four elements are Rx and one is Tx.	Each array is sequentially activated. All US elements are transceivers.	Each element is sequentially activated. All US elements are transceivers.	All are simultaneously activated. All US elements for Tx and Rx
Excitation signal (peak-peak amplitude)	-145V	80V	unknown	up to 50V	-155V	20V
Signal format	Uncoded pulse	Uncoded pulse	Frequency-modulated pulses	Uncoded sine	Uncoded pulse	Modulated Barker-Code sine
Fractional bandwidth of transducer [$]	16% (-3dB)	unknown	100% for Tx 140% for Rx	73% (-6dB)	57.6% (-6dB)	17% (-3dB)
Center frequency	2.2MHz	2.2MHz	10MHz for Tx 4.3MHz for Rx	3.5MHz	3.9MHz	1.95MHz
Flexibility	Inflexible	Inflexible	Inflexible	flexible	flexible	flexible
Mean absolute percentage error [*]	5.3%	-	-	-3.2%	9.4%	-
Classification of bladder filling status [#]	-	Sensitivity = 0.89 Specificity = 0.93	Sensitivity = 0.99 Specificity = 0.995	-	-	Precision = 0.957 Recall = 0.958
Sensor placement protocol	Guided by an additional US imaging device	Guided by a manual placement marker	Sensors are pre-installed to undergarments which are custom made to fit to a subject's body.	By visual inspection assisted by the built-in imaging function of the system	unknown	Sensor-assisted pubic bone detection
Tolerance to misplacement	None	None	None	None	None	± 4.5mm

[&] Including one additional element for pubic bone sensing

[$] Fractional bandwidth = $(f_H - f_L) / fc \times 100\%$, where f_H is the upper -3dB/-6dB frequency corner, f_L is the lower -3dB/-6dB frequency corner and fc is the center frequency.

[*] Mean absolute percentage error = (estimated_volume – true_volume) / true_volume × 100%

[#] Both [22] and [24] were from the same authors who chose sensitivity and specificity as performance indicators. We chose to use precision and recall (where recall is the same as sensitivity). Also, we chose precision instead of specificity because we emphasized the accuracy of full bladder predictions. In clinical practice, frequent false alarms can lead to unnecessary anxiety and additional burden to children.

Although the multi-position training strategy is effective, it requires a longer training time and may be somewhat inconvenient to operate. We plan to design a two-dimensional transducer array for acquiring data without moving the transducer array manually in the training period. After that, it can be replaced by a linear array to reduce its size but to achieve as good classification performance as the current design. The proposed sensor system will be a useful front-end for future closed-loop NE management system. For example, it can potentially drive an electrical stimulator to excite the tibial nerves with stimulus current of different frequencies for eliciting or inhibiting purposes [49]. A robust sensor system that is placement insensitive is a major step towards practical usage in home-use environment.

VII. CONCLUSION

There are two main novelties proposed in this work:

1. Low voltage coded pulses are used to excite the US transducer to reduce the excitation voltage significantly compared to other works. The pulse compression technique helps maintain the same SNR even when using low-voltage excitation signal. It also enhances the safety of system. To the best of the authors' knowledge, this is the first time LV coded pulses have been applied for bladder monitoring.
2. Also, to the best of our knowledge, the multiple positions training strategy in the classification of bladder filling status is the first time it has been proposed. The model trained with multiple positions is robust change in probe displacement, which is common in real-world scenarios.

The proposed device is capable of continuous monitoring of a child's bladder filling status and issuing an alert before nocturnal enuresis actually occurs. The device is of significant clinical value for helping with the management of enuresis conditions and promoting the establishment of normal micturition reflex mechanisms in children. Compared with similar devices in the field, the proposed device is of higher safety and lower sensitivity to placement errors.

REFERENCES

[1] T. Nevéus et al., "Management and treatment of nocturnal enuresis—An updated standardization document from the International Children's Continence Society," *J. Pediatr. Urol.*, vol. 16, no. 1, pp. 10–19, Feb. 2020.

[2] X. Z. Wang et al., "The influence of delay elimination communication on the prevalence of primary nocturnal enuresis—A survey from Mainland China," *Neurourol. Urodynamics*, vol. 38, no. 5, pp. 1423–1429, Apr. 2019.

[3] M. Sarabi et al., "Comprehensive review of nocturnal enuresis in children," *J. Pediatrics Rev.*, vol. 10, no. 3, pp. 227–238, Jul. 2022.

[4] R. A. Walker, "Nocturnal enuresis," *Prim. Care*, vol. 46, no. 2, pp. 243–248, Jun. 2019.

[5] C. S. Jørgensen, K. Kamperis, J. V. Walle, S. Rittig, A. Raes, and L. Dossche, "The efficacy of standard urotherapy in the treatment of nocturnal enuresis in children: A systematic review," *J. Pediatric Urol.*, vol. 19, no. 2, pp. 163–172, Apr. 2023.

[6] E. M. Alqannad, A. S. Alharbi, R. A. Almansour, and M. S. Alghamdi, "Alarm therapy in the treatment of enuresis in children: Types and efficacy review," *Cureus*, vol. 13, Aug. 2021, Art. no. e17358.

[7] N. Caswell et al., "Patient engagement in medical device design: Refining the essential attributes of a wearable, pre-void, ultrasound alarm for nocturnal enuresis," *Pharmaceutical Med.*, vol. 34, no. 1, pp. 39–48, Feb. 2020.

[8] D. Fong, A. V. Alcantar, P. Gupta, E. Kurzrock, and S. Ghiasi, "Non-invasive bladder volume sensing for neurogenic bladder dysfunction management," in *Proc. IEEE 15th Int. Conf. Wearable Implant. Body Sensor Netw. (BSN)*, Las Vegas, NV, USA, Mar. 2018, pp. 82–85.

[9] D. Barolet, F. Christiaens, and M. R. Hamblin, "Infrared and skin: Friend or foe," *J. Photochemistry Photobiol. B, Biol.*, vol. 155, pp. 78–85, Feb. 2016.

[10] S. S. Noyori, G. Nakagami, and H. Sanada, "Non-invasive urine volume estimation in the bladder by electrical impedance-based methods: A review," *Med. Eng. Phys.*, vol. 101, Mar. 2022, Art. no. 103748.

[11] G. Araklitis, M. Paganotto, J. Hunter, G. Thiagamoorthy, D. Robinson, and L. Cardozo, "Can we replace the catheter when evaluating urinary residuals?" *Neurourol. Urodynamics*, vol. 38, no. 4, pp. 1100–1105, Mar. 2019.

[12] H. P. Dietz, D. Velez, K. L. Shek, and A. Martin, "Determination of postvoid residual by translabial ultrasound," *Int. Urogynecol. J.*, vol. 23, no. 12, pp. 1749–1752, May 2012.

[13] M. Dicuio et al., "Measurements of urinary bladder, volume: Comparison of five ultrasound calculation methods in volunteers," *Archivio Italiano di Urologia e Andrologia*, vol. 77, no. 1, pp. 2–60, Mar. 2005.

[14] P. G. van Leuteren, B. A. de Vries, G. C. J. de Joode-Smink, B. ten Haken, T. P. V. M. de Jong, and P. Dik, "URIKA, continuous ultrasound monitoring for the detection of a full bladder in children with dysfunctional voiding: A feasibility study," *Biomed. Phys. Eng. Exp.*, vol. 3, no. 1, Feb. 2017, Art. no. 017005.

[15] H. Niu et al., "Design of an ultrasound bladder volume measurement and alarm system," in *Proc. 5th Int. Conf. Bioinf. Biomed. Eng.*, Wuhan, China, May 2011, pp. 1–4.

[16] J. Zhong et al., "Ultrasound estimation of female bladder volume based on magnetic resonance modeling," *J. Urol.*, vol. 183, no. 1, pp. 216–220, Jan. 2010.

[17] P. Palanchon, D. van Loon, C. H. Bangma, and N. Bom, "Bladder volume measurements with a limited number of fixed ultrasound beams," *Ultrasound Med. Biol.*, vol. 30, no. 3, pp. 289–294, Mar. 2004.

[18] R. Tanaka and T. Abe, "Measurement of the bladder volume with a limited number of ultrasonic transducers," in *Proc. IEEE Int. Ultrason. Symp.*, San Diego, CA, USA, Oct. 2010, pp. 1783–1786.

[19] N. K. Kristiansen, J. C. Djurhuus, and H. Nygaard, "Design and evaluation of an ultrasound-based bladder volume monitor," *Med. Biol. Eng. Comput.*, vol. 42, no. 6, pp. 762–769, Nov. 2004.

[20] H. G. Jo et al., "Forward-looking ultrasound wearable scanner system for estimation of urinary bladder volume," *Sensors*, vol. 21, no. 16, p. 5445, Aug. 2021.

[21] A. C. Kuzmic, B. Brkljacic, and D. Ivankovic, "The impact of bladder shape on the ultrasonographic measurement of bladder volume in children," *Pediatric Radiol.*, vol. 33, no. 8, pp. 530–534, Aug. 2003.

[22] K. Kuru, D. Ansell, M. Jones, C. De Goede, and P. Leather, "Feasibility study of intelligent autonomous determination of the bladder voiding need to treat bedwetting using ultrasound and smartphone ML techniques," *Med. Biol. Eng. Comput.*, vol. 57, no. 5, pp. 1079–1097, May 2019.

[23] K. Kuru et al., "Intelligent autonomous treatment of bedwetting using non-invasive wearable advanced mechatronics systems and MEMS sensors," *Med. Biol. Eng. Comput.*, vol. 58, no. 5, pp. 943–965, May 2020.

[24] K. Kuru et al., "Treatment of nocturnal enuresis using miniaturised smart mechatronics with artificial intelligence," *IEEE J. Transl. Eng. Health Med.*, vol. 12, pp. 204–214, 2024.

[25] L. Jiang et al., "Ultrasound-induced wireless energy harvesting for potential retinal electrical stimulation application," *Adv. Funct. Mater.*, vol. 29, no. 33, May 2019, Art. no. 1902522.

[26] O. Siljama, T. Koskinen, O. Jessen-Juhler, and I. Virkkunen, "Automated flaw detection in multi-channel phased array ultrasonic data using machine learning," *J. Nondestruct. Eval.*, vol. 40, no. 3, pp. 1–13, Aug. 2021.

[27] T. Misaridis and J. A. Jensen, "Use of modulated excitation signals in medical ultrasound. Part I: Basic concepts and expected benefits," *IEEE Trans. Ultrason., Ferroelectr., Freq. Control*, vol. 52, no. 2, pp. 177–191, Feb. 2005.

[28] S. Hedayatrasa, G. Poelman, J. Segers, W. Van Paepegem, and M. Kersemans, "Performance of frequency and/or phase modulated excitation waveforms for optical infrared thermography of CFRPs through thermal wave radar: A simulation study," *Compos. Struct.*, vol. 225, Oct. 2019, Art. no. 111177.

[29] E. Vienneau and B. Byram, "Compound barker-coded excitation for increased signal-to-noise ratio and penetration depth in transcranial ultrasound imaging," in *Proc. IEEE Int. Ultrason. Symp. (IUS)*, Las Vegas, NV, USA, Sep. 2020, pp. 1–4.

[30] K. D. Rao and M. K. Swamy, *Digital Signal Processing: Theory and Practice*. Cham, Switzerland: Springer, 2018.

[31] K. K. Parhi and M. Ayinala, "Low-complexity Welch power spectral density computation," *IEEE Trans. Circuits Syst. I, Reg. Papers*, vol. 61, no. 1, pp. 172–182, Jan. 2014.

[32] J. S. Mattoon and T. G. Nyland, "Fundamentals of diagnostic ultrasound," in *Elsevier eBooks*. St. Louis, MO, USA: Elsevier, 2015, pp. 1–49.

[33] C. Decaro et al., "Machine learning approach for prediction of hematic parameters in hemodialysis patients," *IEEE J. Transl. Eng. Health Med.*, vol. 7, pp. 1–8, 2019.

[34] E. Porter, A. Raterink, and A. Farshkaran, "Microwave-based detection of the bladder state as a support tool for urinary incontinence [bioelectromagnetics]," *IEEE Antennas Propag. Mag.*, vol. 64, no. 1, pp. 112–122, Feb. 2022.

[35] D. Vimalajeewa, E. McDonald, M. Tung, and B. Vidakovic, "Parkinson's disease diagnosis with gait characteristics extracted using wavelet transforms," *IEEE J. Transl. Eng. Health Med.*, vol. 11, pp. 271–281, 2023.

[36] P. Fechner, F. König, W. Kratsch, J. Lockl, and M. Röglinger, "Near-infrared spectroscopy for bladder monitoring: A machine learning approach," *ACM Trans. Manage. Inf. Syst.*, vol. 14, no. 2, pp. 1–23, Jan. 2023.

[37] H. Lee et al., "Efficient sparse coding algorithms," in *The MIT Press eBooks*. Cambridge, MA, USA: MIT Press, 2007, pp. 801–808.

[38] H. T. Lotz, M. van Herk, A. Betgen, F. Pos, J. V. Lebesque, and P. Remeijer, "Reproducibility of the bladder shape and bladder shape changes during filling," *Med. Phys.*, vol. 32, no. 8, pp. 2590–2597, Jul. 2005.

[39] S. R. Bolla et al., *Histology, Bladder*. St. Petersburg, FL, USA: StatPearls Publishing, 2021.

[40] S. B. Bauer, R. J. M. Nijman, B. A. Drzewiecki, U. Sillen, and P. Hoebeke, "International children's continence society standardization report on urodynamic studies of the lower urinary tract in children," *Neurourol. Urodynamics*, vol. 34, no. 7, pp. 640–647, May 2015.

[41] S. Mattsson, D. Persson, G. Glad Mattsson, and S. Lindström, "Night-time diuresis pattern in children with and without primary monosymptomatic nocturnal enuresis," *J. Pediatric Urol.*, vol. 15, no. 3, pp. 229.e1–229.e8, May 2019.

[42] L. Zhang et al., "A conformable phased-array ultrasound patch for bladder volume monitoring," *Nature Electron.*, vol. 7, no. 1, pp. 77–90, Nov. 2023.

[43] C. Wang et al., "Bioadhesive ultrasound for long-term continuous imaging of diverse organs," *Science*, vol. 377, no. 6605, pp. 517–523, Jul. 2022.

[44] C. Pu, B. Fu, L. Guo, H. Xu, and C. Peng, "A stretchable and wearable ultrasonic transducer array for bladder volume monitoring application," *IEEE Sensors J.*, vol. 24, no. 10, pp. 15875–15883, May 2024.

[45] E. Dunne, A. Santorelli, B. McGinley, G. Leader, M. O'Halloran, and E. Porter, "Supervised learning classifiers for electrical impedance-based bladder state detection," *Sci. Rep.*, vol. 8, no. 1, pp. 1–12, Mar. 2018.

[46] P. H. Gopalakrishnan and M. R. Panicker, "Non-Newtonian fluid coupling media for wearable ultrasound imaging systems using rigid linear sensor array," *Sens. Actuators A, Phys.*, vol. 376, Oct. 2024, Art. no. 115588.

[47] S. Li and B. Zhang, "Joint discriminative sparse coding for robust hand-based multimodal recognition," *IEEE Trans. Inf. Forensics Security*, vol. 16, pp. 3186–3198, 2021.

[48] P. Ghaderyan and A. Abbasi, "Sparse coding classification and cepstral singular value for cognitive workload estimation," *Comput. Electr. Eng.*, vol. 91, May 2021, Art. no. 107031.

[49] X. Li et al., "Efficacy of a novel wearable transcutaneous tibial nerve stimulation device on bladder reflex compared to implantable tibial nerve stimulation in cats," *Int. Urol. Nephrol.*, vol. 55, no. 4, pp. 853–859, Dec. 2022.

[50] T. Keten et al., "Comparison of the efficacy of desmopressin fast-melting formulation and enuretic alarm in the treatment of monosymptomatic nocturnal enuresis," *J. Pediatric Urol.*, vol. 16, no. 5, pp. 645.e1–645.e7, Oct. 2020.